GSA Data Repository 2019197

Chamberlin, E.P., and Hajek, E.A., 2019, Using bar preservation to constrain reworking in channel-dominated fluvial stratigraphy: Geology, https://doi.org/10.1130/G46046.1

# SUPPLEMENTAL INFORMATION

## DATA FROM THE CASTLEGATE SANDSTONE

### Site selection

Bar preservation was classified in three outcrop panels in the lower Castlegate Sandstone along the Wasatch Plateau (Figure 2 and Figure DR1). The outcrops used in this study are oblique to paleoflow direction, and flow direction of individual bars can vary widely; paleoflow at Price and Joe's Valley was east-southeast (Robinson and Slingerland, 1998), and southeast at Salina (Chamberlin, 2016). The analyzed outcrop panels are at least three times the observed average bar width and eight times measured average paleoflow depths.

Gigapans (high resolution photo panoramas) for each panel are available online at the following locations:

1) Price Canyon panel: http://www.gigapan.com/gigapans/181311
2) Joe's Valley: http://www.gigapan.com/gigapans/177202
3) Salina Canyon: http://www.gigapan.com/gigapans/175868

Terrestrial lidar datasets of the Price and Salina Canyon panels are available from the authors.

Figure DR1 (next pages): Castlegate outcrop panel locations (yellow) shown on Google Earth images. Polygons are available as a KML file at the following location: https://sites.google.com/a/denison.edu/supplement_chamberlin_hajek/. Blue arrows show published mean paleocurrent directions for Price (A; 102.9°) and Joe's Valley (B; 127.5°) (Robinson and Slingerland, 1998). Authors' mean paleocurrent direction is shown for Salina (C; 132°), which contrasts with previously published measurements from Adams and Bhattacharya (2005) that show a southwest mean paleocurrent direction in the same area.

**A.** Price Panel location near the type section at Castle Gate (central location: N 39° 44’ 55.81’’, W 110° 52’ 50.05’’.

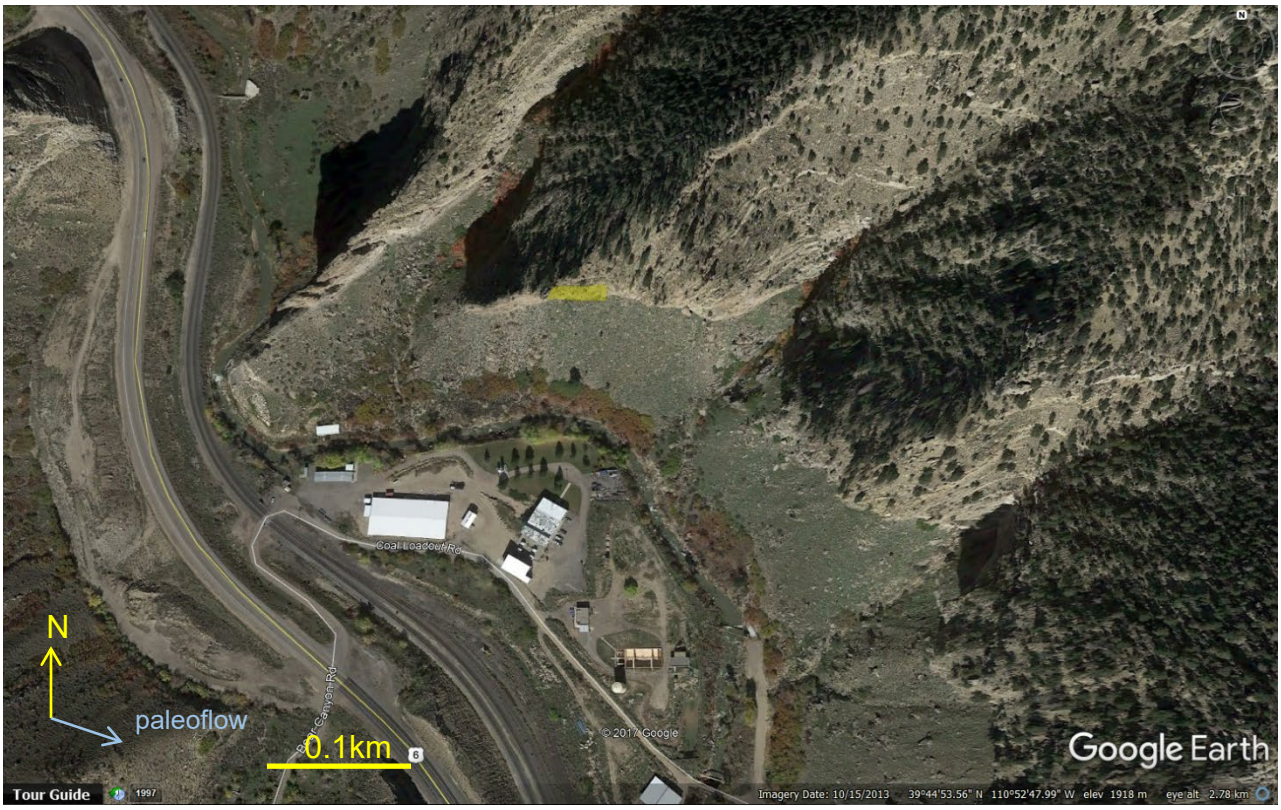


**B.** Joe’s Valley panel location along the road bordering the reservoir (central location: N 39° 17’ 41.55’’, W 111° 16’ 16.94’’).

**C.** Salina Canyon panel location along Water Hollow Road (central location: N 38° 54’ 07.83’’, W 111° 39’ 19.82’’).

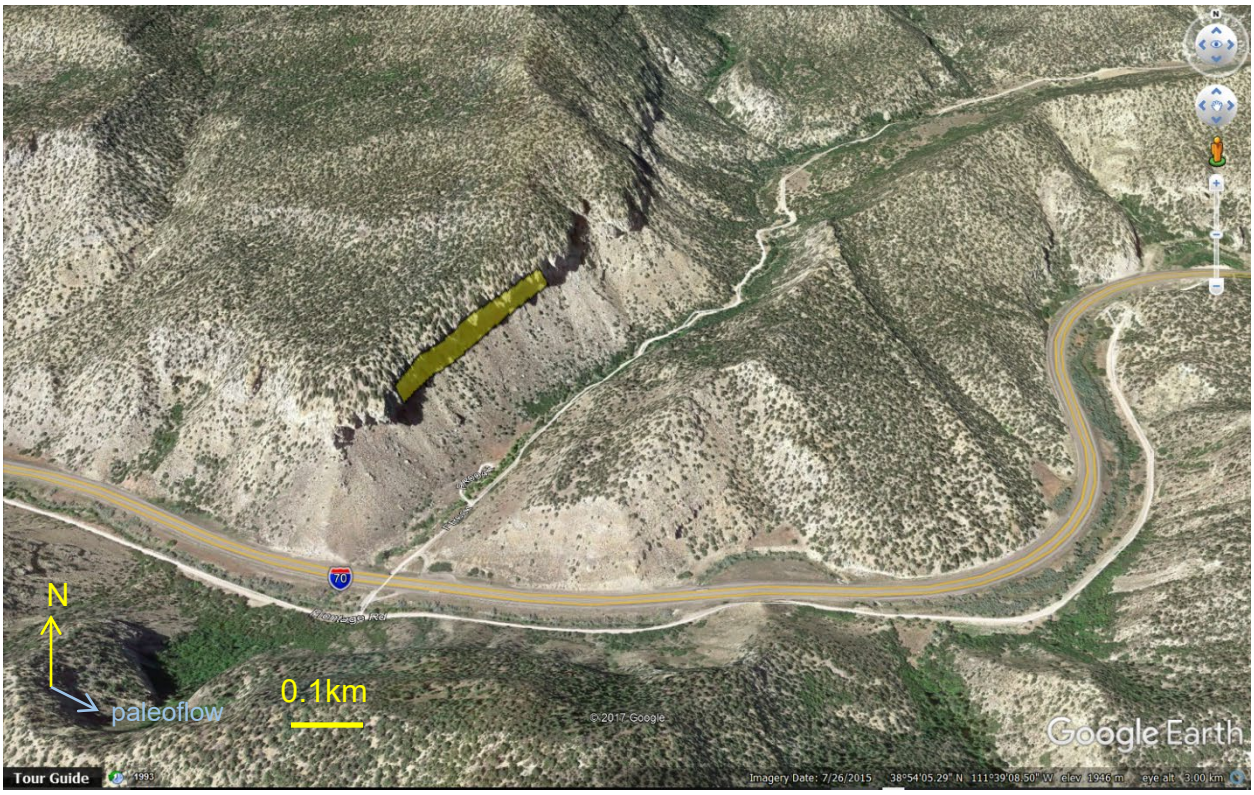

**Mapping bar preservation**

We used a combination of detailed field observations, Gigapans (high resolution photo panoramas), and terrestrial lidar (laser-generated 3D outcrop models) to evaluate bar preservation at each site. Figures DR2 – DR4 on the following pages show high-resolution, enlarged versions of each mapped panel.

To categorize bar preservation at each outcrop, we began with using field observations, measured sections, and high-resolution imagery to map lithofacies and scour surfaces on the outcrop panels. Table DR1 contains summary lithofacies descriptions at each site. To separate the effects of channel avulsion from intra-channel-belt dynamics, we categorized scour surfaces as channel-belt or intra-channel-belt, following Chamberlin and Hajek (2015). Channel belt scours were laterally extensive and were stratal termination surfaces for smaller-scale scours; these are approximately equivalent to the SRS 7-scale surfaces of Miall (2014). Intra-channel-belt scours had limited lateral extent, terminated against other intra-channel-belt scours or channel-belt scours, and often had smaller vertical relief.

These lithofacies and scour surface maps become the basis for mapping bar surfaces and interpreting bar cosets. Bar clinoform sets were identified as successive ($\geq$3) clinothem packages that have similar dip, geometry, thickness, and facies characteristics. We identified bar packages as inclined, sigmoidal, or dome-shaped clinoforms within channel/bar facies that shared dip directions and stratal termination surfaces (e.g., onlap, downlap, or truncation). Finally, we categorized each bar coset as fully, partially, or poorly preserved based on the geometry and lithofacies criteria defined in the manuscript. After interpreting the preservation of each bar coset, we identified bars that directly underlie channel-belt scours, because these large-scale scours are driving the landscape reworking at the stratigraphic architecture scale.

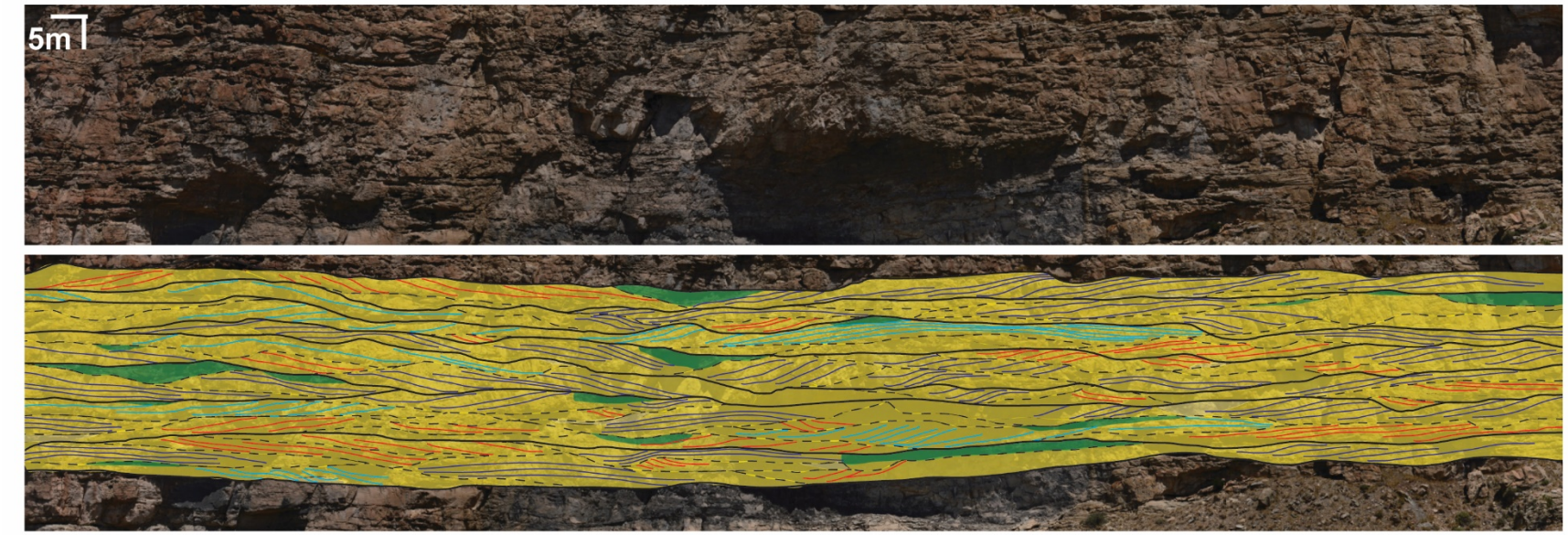


Figure DR2: Enlarged panel of lithofacies and bar preservation from Price Canyon. The panel is oriented east-west (Figure DR1a). See manuscript Figure 2 for key and explanation.

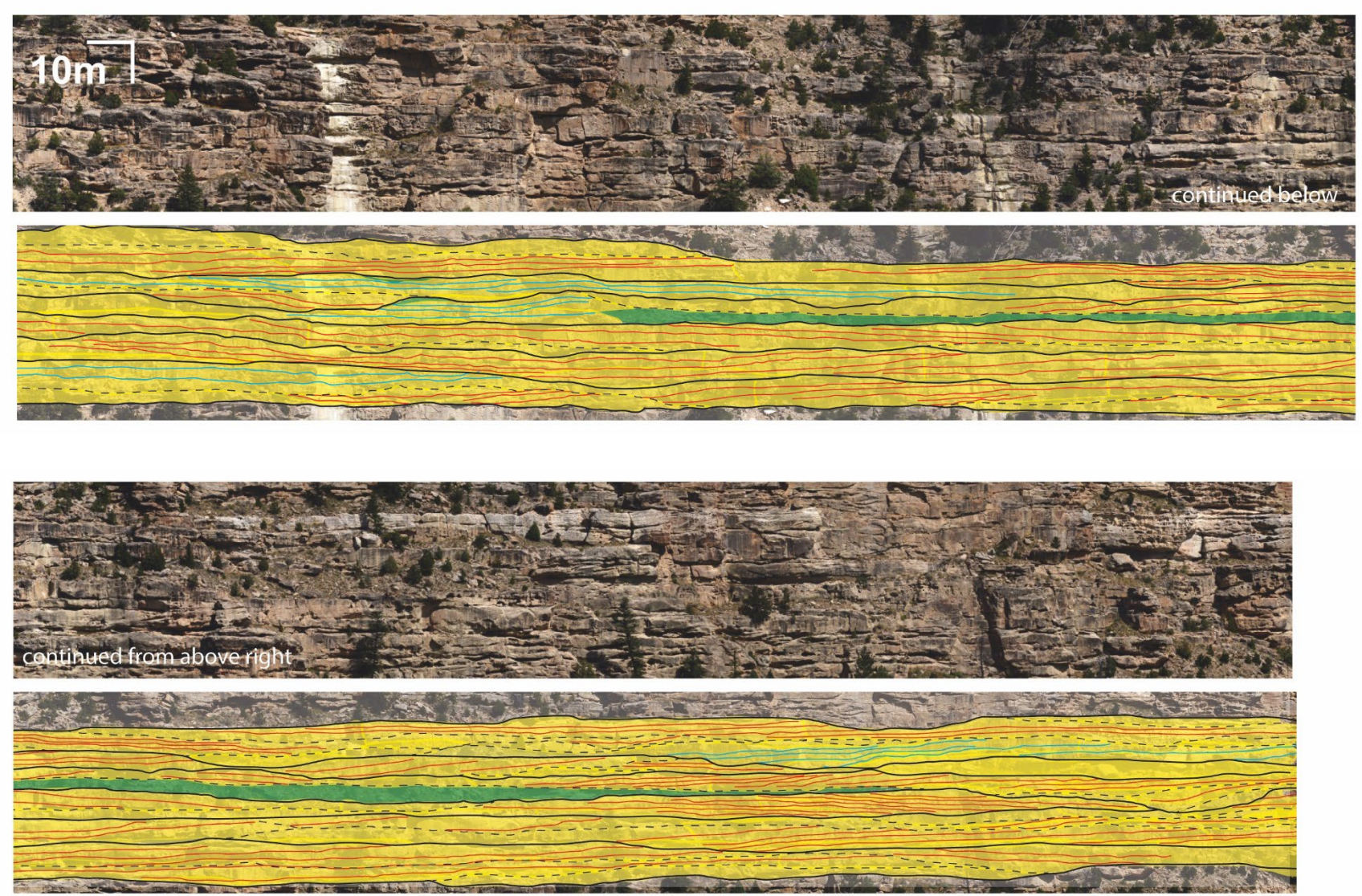


Figure DR3: Enlarged panel of lithofacies and bar preservation from Joe's Valley. The panel is oriented north-south (Figure DR1b). See manuscript Figure 2 for key and explanation.

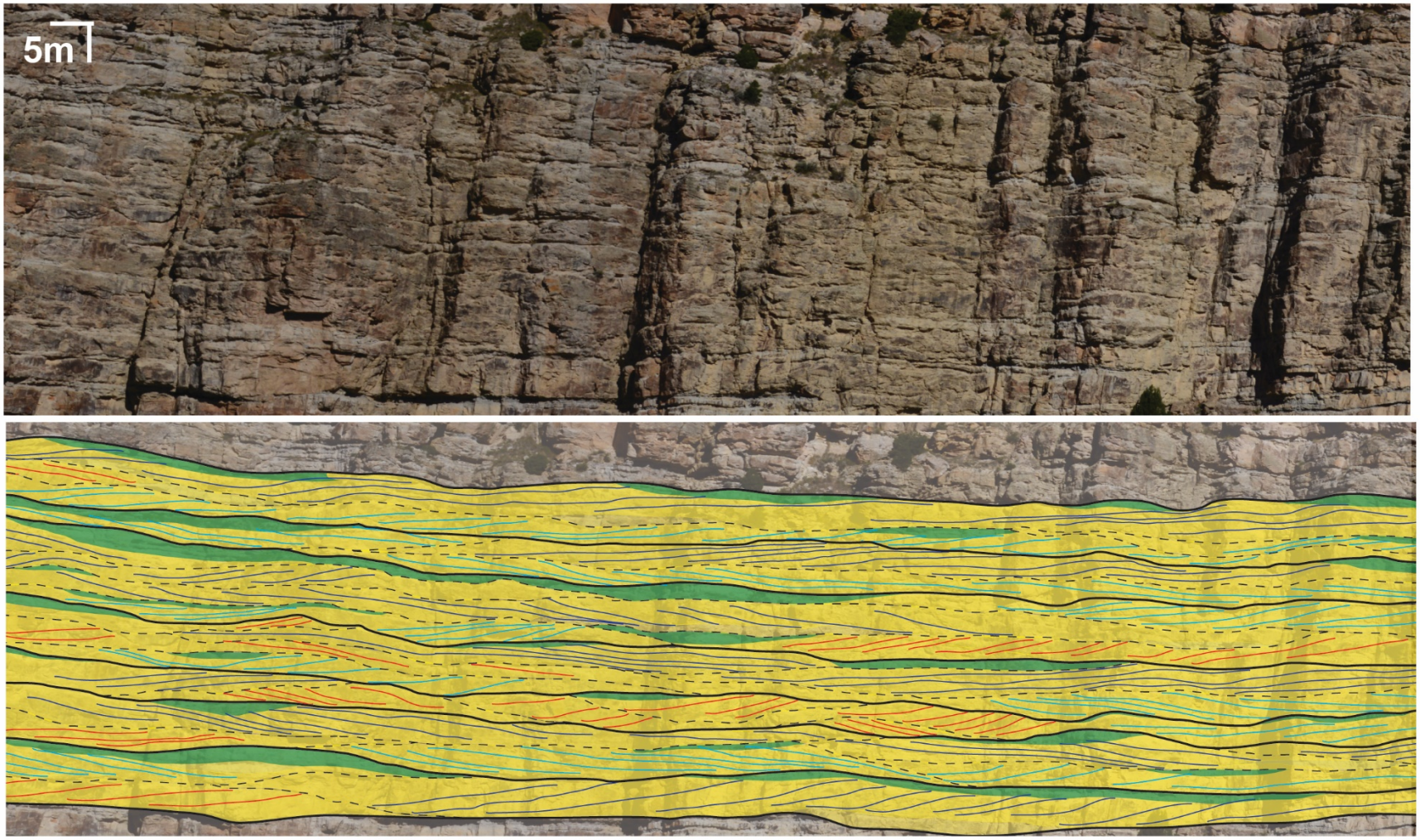


Figure DR4: Enlarged panel of bar preservation and lithofacies from Salina Canyon. The panel is oriented north-northeast-south-southwest (Figure DR1c). See manuscript Figure 2 for key and explanation.

Table DR1: Castlegate lithofacies summary.

| | Price Canyon | Joe's Valley | Salina Canyon |
|---|---|---|---|
| **Bar** | Normally graded upper medium to lower fine sandstone with 0.1-0.5m thick trough cross-stratification sets and soft sediment deformation. Bedsets have sharp bases with some mud rip-up clasts. Many bar packages contain pockets of organic-rich, rippled, thinly bedded very fine sand at the bar toes. Lenses of upper medium trough cross-stratified thalweg deposits are present but rare. | Upper fine sandstone to granules with 0.1-1m thick trough cross-stratification sets and highly amalgamated beds. Beds (0.2-0.5m thick) with very coarse sand to pebble bases commonly grade upward into upper fine sand. Beds have sharp bases with common gray/white silt rip-up clasts. Lenses of fine lower sand at bar toes are rare. | Lower fine to upper medium-grained sandstone with organized 0.1-0.75m thick trough cross-stratification sets and some low-angle parallel laminations. Bedsets have sharp bases with rare granule lenses, and some contain soft sediment deformation. At the toes of some bar packages, there are centimeter- to decimeter-scale lenses of silt to lower fine sandstone with climbing and current ripples, parallel laminae, and organic matter drapes. |
| **Bar top** | Heavily rippled very fine sandstone gradational with underlying bar facies. Occasionally grades upward into massive gray siltstone. Lithofacies is up to 1.5m thick with 0.1-0.5m thick beds. Organic-rich laminae are abundant. | 0.2-0.6m thick beds of upper very fine to lower medium sandstone containing less than 0.1m thick sets of trough and tabular cross-stratification and current ripples. Beds are gradational with underlying bar lithofacies and are laterally discontinuous. | Decimeter- to meter-scale very fine lower to fine lower, thinly bedded, rippled sandstone with interbeds of gray siltstone. Sandstone interbeds are 0.1-0.5m thick with small-scale current ripples, some climbing ripples, organic laminae, parallel laminations, and soft sediment deformation, and are interbedded with 0.1-0.2m thick siltstone beds. Bedsets are gradational with underlying bar facies, and the upper contact ranges from gradational to truncated. |
| **Overbank and abandon-ment** | Thinly bedded to massive gray siltstone and very fine lower sandstone with abundant organic material and limited paleosol development. | Thin (less than 0.2m thick) lower very fine sand beds with ripples and root casts interbedded with laminated to massive dark gray mudstone. | Decimeter- to meter-scale laminated gray siltstone and interbedded very fine lower to very fine upper sandstone. Sandstone beds have vertical root traces and are massive to parallel laminated. These deposits have aggradational basal contacts and erosional upper contacts. |

**Time-equivalence of study sites**

The upper Campanian Castlegate Sandstone comprises three informal units within the Mesaverde Group: the amalgamated lower Castlegate Sandstone (the subject of this study), the heterolithic middle Castlegate, and the coarse-grained Bluecastle Tongue (Fouch et al., 1983; McLaurin and Steel, 2000). The age and correlation of the lower Castlegate Sandstone has been a subject of extensive study and debate. Our Price Canyon outcrop location is in the same cliff face as the type section at Castle Gate, where the stratigraphy of the lower interval as lower Castlegate Sandstone is universally agreed upon (McLaurin and Steel, 2000; Miall and Arush, 2001; Pattison, 2010; Robinson and Slingerland, 1998; Van Wagoner, 1995; Yoshida, 2000; Yoshida et al., 1996). At Joe's Valley, however, the age of the basal quartz sandstone interval is debated. Robinson and Slingerland (1998) used palynology, lithofacies observations, and paleocurrent indicators to correlate the quartz sandstone at Joe's Valley with the lower Castlegate Sandstone in Price Canyon. In contrast, Miall and Arush (2001) use sandstone petrography to correlate the Joe's Valley sandstone with the younger Bluecastle Tongue, the unit overlying the lower Castlegate. These authors suggest that the base-Bluecastle unconformity has removed all lower Castlegate-age deposition from Joe's Valley. Neither of these interpretations is definitive, but as Miall and Arush (2001) acknowledge, small differences in sandstone petrology may record variations in source terrane along the Wasatch Plateau, rather than chronostratigraphic differences. For that reason, we use Robinson and Slingerland (1998)'s correlation in this study, as it is based on more concrete palynological evidence and field observations. Finally, the subdivisions of the Castlegate Sandstone are not traceable to the Salina Canyon site in the southern Wasatch Plateau, but we follow previous authors in the assumption that the quartz-rich amalgamated unit directly overlying the Blackhawk Formation is the lower Castlegate Sandstone (Adams and Bhattacharya, 2005). Overall, then, the exact age-equivalence between the sites in this study is not confidently established. However, at each of these sites, we examined the amalgamated quartz arenite unit directly overlying the mud-dominated fluvial Blackhawk Formation; as such, the previously interpreted change from high to low accommodation-creation has been assumed at all three sites.

## OBJECT-BASED MODEL DESIGN AND SETUP

The model used in this study is a 2D rule-based model modified from Chamberlin and Hajek (2015); see that reference for more details on model parameters and behaviors. This simple model builds stratigraphy with rectangular "channel elements" and floodplain deposits that are placed into the model basin at each timestep according to a set of avulsion and aggradation rules for determining the channel element location and floodplain aggradation. In the "random avulsion" case, the channel element location is drawn from a uniform random distribution of locations across the model domain. In the "compensational avulsion" case, the channel element is placed at the lowest point in the model domain (if there are multiple points of the same elevation, the location is selected randomly from the lowest points), and every $10^{th}$ timestep is a randomly selected avulsion location.

Basin topography is updated at each timestep once an avulsion location is chosen. The channel height, or location along the y-axis, is determined as a function of the pre-existing topographic height plus the channel-element thickness minus the channel-element incision (where incision is a proportion of the channel thickness), and floodplain locations aggrade following an exponential decay function on each side of the channel element. Floodplain does not aggrade above the height of the active channel element. The total amount of channel vs. floodplain accumulation is set by the ratio of the channel element area to the floodplain deposit area per timestep. The channel element area is set by the channel dimensions and is constant throughout the model run; the floodplain deposit area is set by the floodplain aggradation rate and also can vary per timestep according to the pre-existing topography, because floodplain does not aggrade above the height of the active channel element. Together, the input ratio of channel and floodplain input and the channel incision determine the overall model aggradation rate (where high floodplain aggradation rates and low channel incision yields the highest model aggradation rate).

Over 100s of timesteps, these topography and location rules generate model stratigraphy with channel objects that have measurable preservation (Figure DR5, DR6). To calculate channel element preservation, we categorized channel elements as well preserved or poorly preserved based on maximum vertical preservation (MVP; Figure DR5) and total area preserved (TA; Figure DR5). Well preserved channel elements have retained their original thickness at some point along their width and have at least 50% of the total area preserved. Remaining elements are categorized as poorly preserved. The "well preserved" model category is roughly analogous to both the fully preserved and partially preserved field categories, and the poorly preserved model category approximates the "poorly preserved" field classification.

The net-to-gross of the model output is the percent of the output area that is channel element (i.e., the percent sand). Sediment retention (the fraction of supplied sediment retained in the final cross-section) is the final output area divided by the sum of the floodplain and channel input areas, which ultimately acts as a measure of how much of the total sediment input is preserved in the model stratigraphy.

For all runs, channel elements are 2.6 model units high and 119 model units wide, in a model domain that is 50 times the channel element width (Figure DR6). Each run is 1000 timesteps, which generates thick enough output that the "outcrop analysis" window falls in the center of the stratigraphy and does not include either the first or last 10% of channel elements to allow for model spin-up time and to avoid fully preserved elements at the top of the model output. The exponent for the exponential decay of floodplain aggradation away from the channel is -0.005 for all runs. Table DR2 shows additional model input parameters and results for each run included in this study. Model parameters can be scaled to different formations and outcrops, and Monte Carlo sampling of modeled stratigraphy can be used to establish the range of preservation that might be expected in outcrops of different sizes and with different numbers of exposed channel elements (e.g., Trampush et al., 2017).

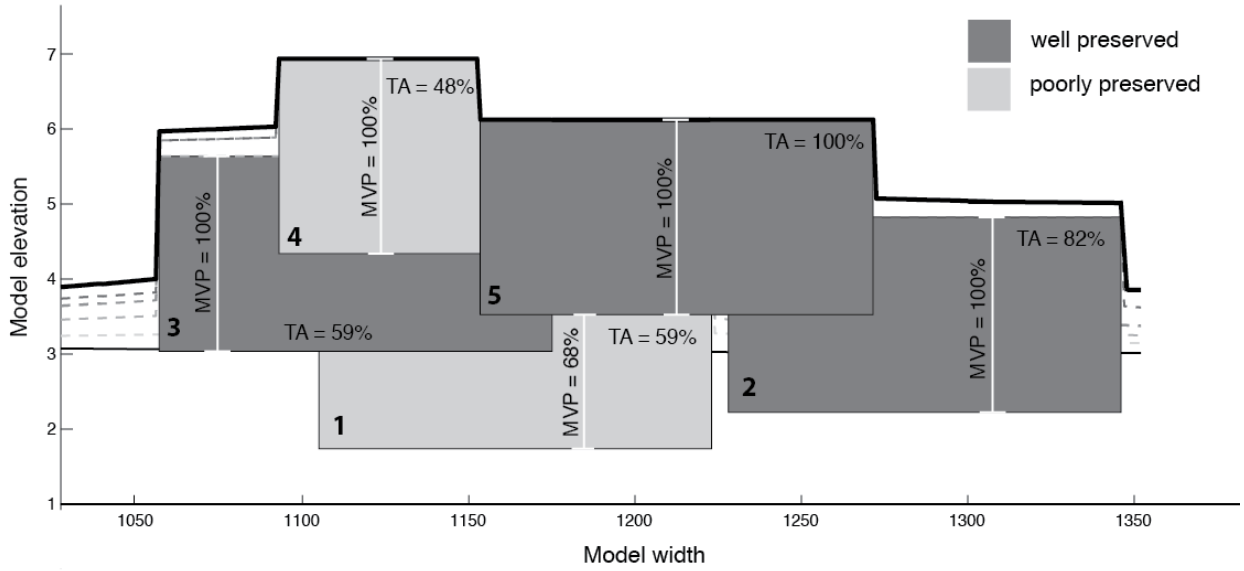


Figure DR5: Example 2D geometric model output for a random avulsion model run with a channel incision rate of 50% of the channel-element thickness and a floodplain aggradation rate of 12.5% of the channel-element thickness per timestep. Each rectangle is a channel element, and the numbers in the bottom left corner of each element indicate their relative age (1 being the oldest channel, 5 being the youngest). Elements with maximum vertical preservation (MVP) >99% and total area (TA) >50% are classified as well preserved (dark gray), while elements with MVP <99% or TP <50% are classified as poorly preserved (light gray). Dashed lines indicate floodplain topography at each timestep, and the bold black line indicates the final topography.

Figure DR6 (next pages): Examples of avulsion model outputs for runs with a range of bar preservations for random (A-B) and compensational (C-D) avulsions, including a full model output (top) and zoomed in model output of a subsection of the same run (bottom) for each example. Colors represent timestep from oldest (dark) to youngest (light). Black lines show topography for each timestep. In (A) top, the black rectangle delineates an area analogous to an outcrop-sized window within which the channel element preservation is analyzed.

A. Random avulsion model output with high bar preservation (run 3 in Table DR2)

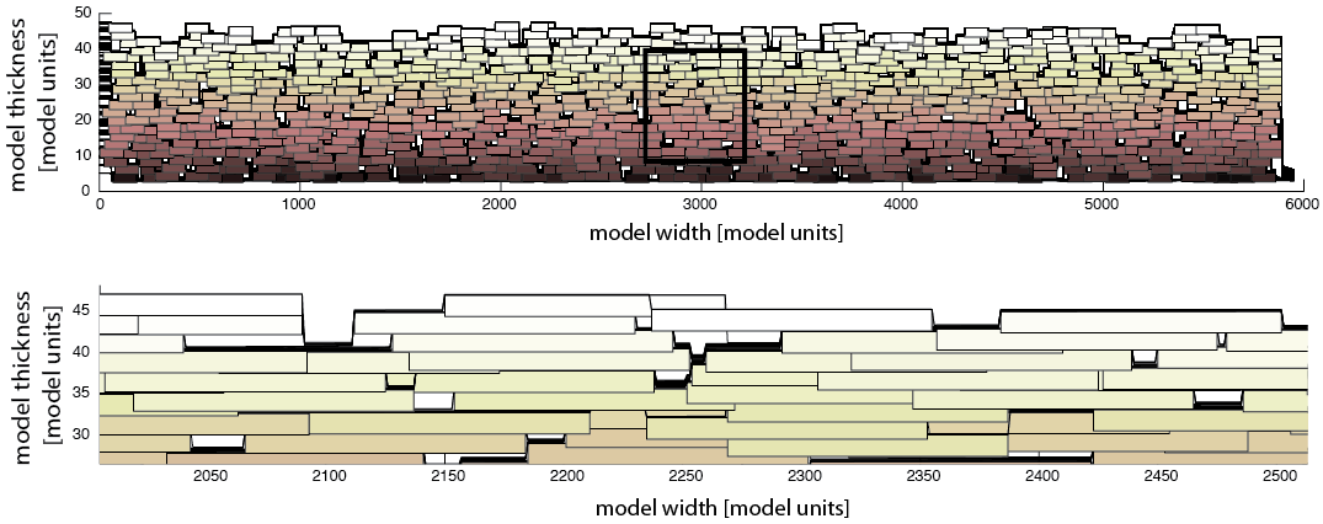


B. Random avulsion model output with low bar preservation (run 33 in Table DR2)

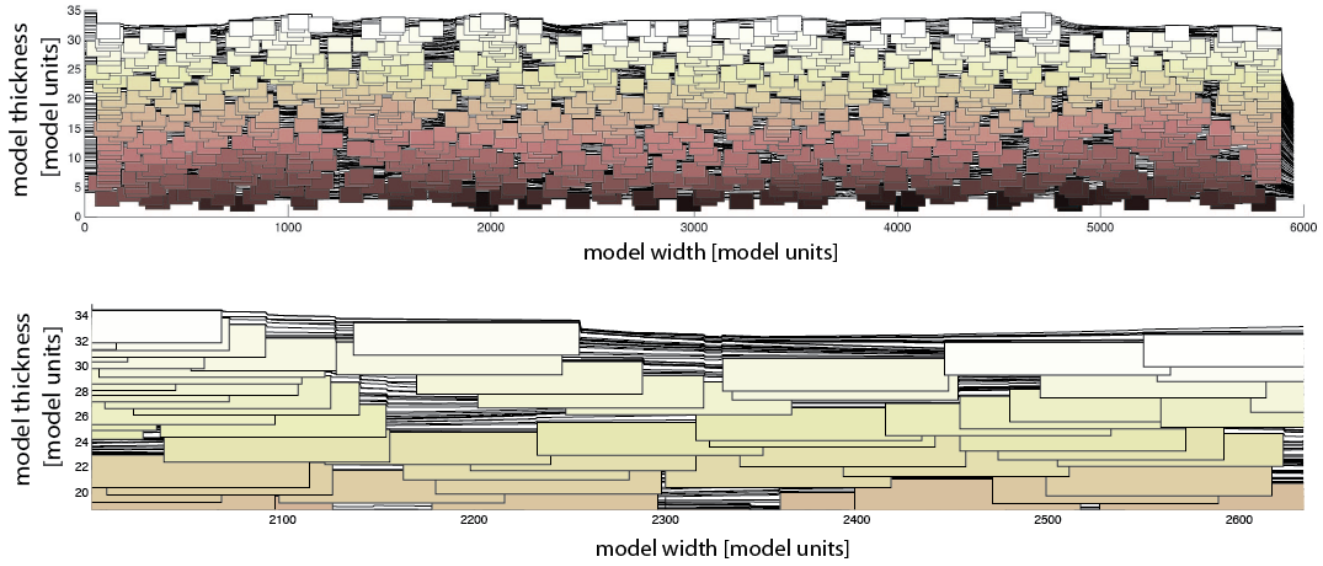

C. Compensational avulsion model output with high bar preservation (run 2 in Table DR2)

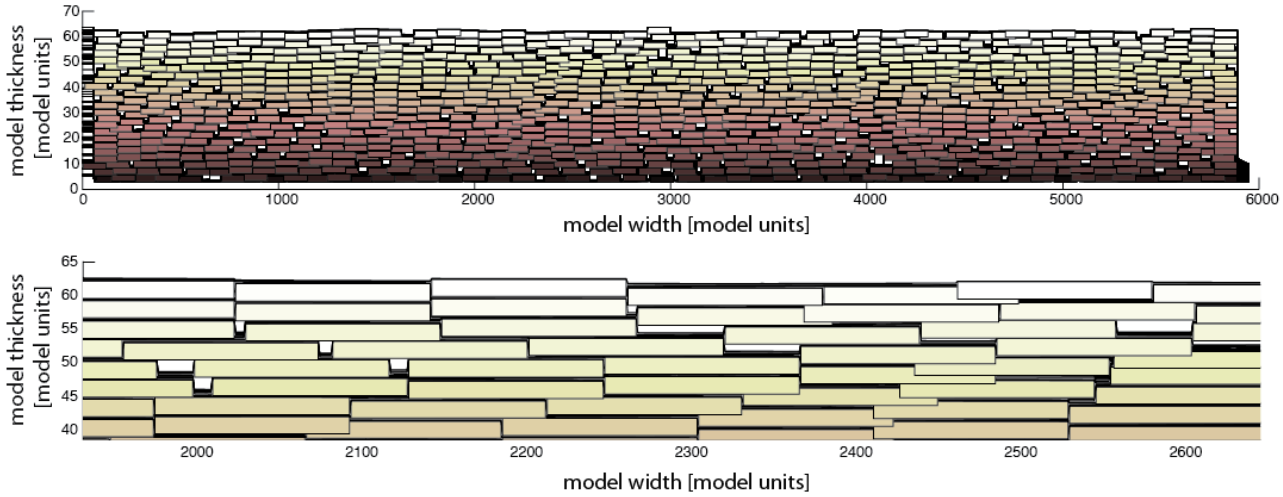


D. Compensational avulsion model output with low bar preservation (run 35 in Table DR2)

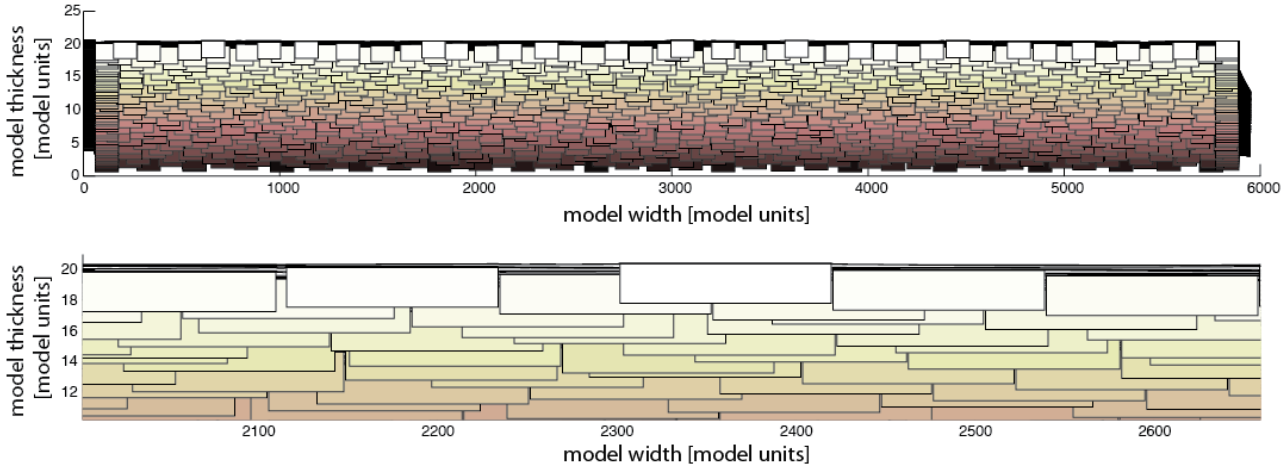

Table DR2: Input parameters and results for model runs in this study. See text for variable descriptions.

| Run # | Incision rate [% channel depth] | Floodplain aggradation [model units] | Ratio of overbank to channel input | Well preserved bars [%] | Poorly preserved bars [%] | Net-to-gross [% sand in model output] | Sediment retention [%] |
|---|---|---|---|---|---|---|---|
| Random avulsion pattern | | | | | | | |
| 1 | 10 | 0.1 | 0.09 | 65.0 | 35.0 | 84.8 | 86.4 |
| 2 | 10 | 0.2 | 0.19 | 88.6 | 11.4 | 85.7 | 89.4 |
| 3 | 20 | 0.1 | 0.09 | 52.1 | 47.9 | 94.8 | 79.4 |
| 4 | 20 | 0.2 | 0.18 | 60.0 | 40.0 | 89.8 | 83.5 |
| 5 | 20 | 0.3 | 0.28 | 93.9 | 6.1 | 83.1 | 85.8 |
| 6 | 30 | 0.1 | 0.09 | 54.3 | 45.7 | 91.8 | 72.8 |
| 7 | 30 | 0.2 | 0.18 | 66.7 | 33.3 | 87.7 | 76.8 |
| 8 | 30 | 0.3 | 0.27 | 73.8 | 26.2 | 85.4 | 79.3 |
| 9 | 30 | 0.4 | 0.36 | 78.1 | 21.9 | 80.4 | 81.0 |
| 10 | 40 | 0.1 | 0.09 | 40.8 | 59.2 | 95.9 | 66.3 |
| 11 | 40 | 0.1 | 0.17 | 62.5 | 37.5 | 88.9 | 69.4 |
| 12 | 40 | 0.2 | 0.27 | 78.6 | 21.4 | 85.1 | 72.6 |
| 13 | 50 | 0.3 | 0.08 | 32.8 | 67.2 | 97.2 | 57.9 |
| 14 | 50 | 0.1 | 0.17 | 46.7 | 53.3 | 92.4 | 61.8 |
| 15 | 50 | 0.2 | 0.27 | 61.5 | 38.5 | 88.5 | 65.2 |
| 16 | 50 | 0.3 | 0.36 | 71.1 | 28.9 | 82.4 | 67.8 |
| 17 | 50 | 0.4 | 0.47 | 78.4 | 21.6 | 80.6 | 70.4 |
| 18 | 60 | 0.5 | 0.08 | 33.9 | 66.1 | 91.5 | 49.3 |
| 19 | 60 | 0.1 | 0.17 | 26.8 | 73.2 | 89.0 | 53.8 |
| 20 | 60 | 0.2 | 0.27 | 48.0 | 52.0 | 82.6 | 58.1 |
| 21 | 60 | 0.3 | 0.37 | 45.3 | 54.7 | 90.1 | 61.0 |
| 22 | 60 | 0.4 | 0.48 | 56.8 | 43.2 | 81.1 | 64.1 |
| 23 | 70 | 0.5 | 0.08 | 17.7 | 82.3 | 98.4 | 41.6 |
| 24 | 70 | 0.1 | 0.18 | 21.1 | 78.9 | 96.9 | 45.9 |
| 25 | 70 | 0.2 | 0.28 | 31.7 | 68.3 | 92.4 | 50.5 |
| 26 | 70 | 0.3 | 0.38 | 46.7 | 53.3 | 83.9 | 54.4 |
| 27 | 70 | 0.4 | 0.48 | 72.7 | 27.3 | 81.7 | 57.5 |
| 28 | 70 | 0.5 | 0.59 | 72.5 | 27.5 | 80.7 | 60.5 |
| 29 | 70 | 0.6 | 0.68 | 46.9 | 53.1 | 80.4 | 62.7 |
| 30 | 80 | 0.7 | 0.08 | 5.3 | 94.7 | 98.0 | 32.2 |
| 31 | 80 | 0.1 | 0.18 | 12.9 | 87.1 | 95.2 | 37.9 |
| 32 | 80 | 0.2 | 0.29 | 19.7 | 80.3 | 94.8 | 42.8 |
| 33 | 80 | 0.3 | 0.38 | 42.1 | 57.9 | 87.9 | 46.6 |
| 34 | 80 | 0.4 | 0.47 | 50.9 | 49.1 | 89.3 | 50.0 |
| 35 | 80 | 0.5 | 0.56 | 48.0 | 52.0 | 87.2 | 53.0 |
| 36 | 80 | 0.6 | 0.69 | 57.9 | 42.1 | 82.2 | 56.9 |
| 37 | 90 | 0.8 | 0.09 | 3.6 | 96.4 | 94.0 | 22.8 |

| Run # | Incision rate [% channel depth] | Floodplain aggradation [model units] | Ratio of overbank to channel input | Well preserved bars [%] | Poorly preserved bars [%] | Net-to-gross [% sand in model output] | Sediment retention [%] |
|---|---|---|---|---|---|---|---|
| Random avulsion pattern continued | | | | | | | |
| 38 | 90 | 0.1 | 0.18 | 7.7 | 92.3 | 92.6 | 29.4 |
| 39 | 90 | 0.2 | 0.26 | 16.1 | 83.9 | 95.0 | 34.0 |
| 40 | 90 | 0.3 | 0.34 | 33.3 | 66.7 | 86.7 | 37.8 |
| 41 | 90 | 0.4 | 0.39 | 47.1 | 52.9 | 89.1 | 39.9 |
| Compensational avulsion pattern | | | | | | | |
| 1 | 10 | 0.1 | 0.11 | 97.1 | 2.9 | 91.7 | 97.3 |
| 2 | 10 | 0.2 | 0.23 | 100.0 | 0.0 | 89.0 | 97.5 |
| 3 | 20 | 0.1 | 0.11 | 43.9 | 56.1 | 98.0 | 87.9 |
| 4 | 20 | 0.2 | 0.22 | 100.0 | 0.0 | 86.6 | 90.0 |
| 5 | 20 | 0.3 | 0.34 | 100.0 | 0.0 | 80.1 | 90.8 |
| 6 | 30 | 0.1 | 0.11 | 55.8 | 44.2 | 94.7 | 80.7 |
| 7 | 30 | 0.2 | 0.23 | 61.0 | 39.0 | 94.1 | 81.2 |
| 8 | 30 | 0.3 | 0.34 | 97.1 | 2.9 | 87.2 | 83.0 |
| 9 | 40 | 0.1 | 0.11 | 66.0 | 34.0 | 92.9 | 70.2 |
| 10 | 40 | 0.2 | 0.23 | 66.7 | 33.3 | 95.9 | 73.2 |
| 11 | 40 | 0.3 | 0.34 | 89.2 | 10.8 | 92.9 | 75.4 |
| 12 | 40 | 0.4 | 0.46 | 100.0 | 0.0 | 87.5 | 77.1 |
| 13 | 50 | 0.1 | 0.11 | 54.4 | 45.6 | 99.2 | 61.1 |
| 14 | 50 | 0.2 | 0.23 | 60.8 | 39.2 | 97.4 | 65.0 |
| 15 | 50 | 0.3 | 0.34 | 69.2 | 30.8 | 96.7 | 67.7 |
| 16 | 50 | 0.4 | 0.46 | 94.4 | 5.6 | 92.5 | 70.2 |
| 17 | 50 | 0.5 | 0.58 | 100.0 | 0.0 | 85.3 | 72.4 |
| 18 | 60 | 0.1 | 0.11 | 40.4 | 59.6 | 98.2 | 51.9 |
| 19 | 60 | 0.2 | 0.23 | 62.5 | 37.5 | 97.8 | 56.4 |
| 20 | 60 | 0.3 | 0.34 | 57.1 | 42.9 | 96.7 | 60.3 |
| 21 | 60 | 0.4 | 0.46 | 66.7 | 33.3 | 93.7 | 63.4 |
| 22 | 60 | 0.5 | 0.58 | 100.0 | 0.0 | 88.5 | 66.3 |
| 23 | 70 | 0.1 | 0.11 | 16.4 | 83.6 | 99.0 | 42.9 |
| 24 | 70 | 0.2 | 0.23 | 35.0 | 65.0 | 98.3 | 48.0 |
| 25 | 70 | 0.3 | 0.35 | 70.4 | 29.6 | 98.3 | 52.7 |
| 26 | 70 | 0.4 | 0.46 | 86.4 | 13.6 | 94.8 | 56.7 |
| 27 | 70 | 0.5 | 0.58 | 92.3 | 7.7 | 89.2 | 59.9 |
| 28 | 70 | 0.6 | 0.70 | 100.0 | 0.0 | 85.9 | 62.8 |
| 29 | 80 | 0.1 | 0.11 | 5.3 | 94.7 | 99.0 | 33.7 |
| 30 | 80 | 0.2 | 0.23 | 20.8 | 79.2 | 97.3 | 40.1 |
| 31 | 80 | 0.3 | 0.35 | 45.0 | 55.0 | 97.9 | 45.4 |
| 32 | 80 | 0.4 | 0.47 | 74.0 | 26.0 | 96.2 | 49.9 |
| 33 | 80 | 0.5 | 0.58 | 83.7 | 16.3 | 84.4 | 53.6 |

| Run # | Incision rate [% channel depth] | Floodplain aggradation [model units] | Ratio of overbank to channel input | Well preserved bars [%] | Poorly preserved bars [%] | Net-to-gross [% sand in model output] | Sediment retention [%] |
|---|---|---|---|---|---|---|---|
| Compensational avulsion pattern continued | | | | | | | |
| 34 | 90 | 0.1 | 0.11 | 5.2 | 94.8 | 98.4 | 24.6 |
| 35 | 90 | 0.2 | 0.23 | 5.5 | 94.5 | 98.7 | 32.0 |
| 36 | 90 | 0.3 | 0.33 | 26.9 | 73.1 | 90.2 | 37.3 |
| 37 | 90 | 0.4 | 0.40 | 31.1 | 68.9 | 80.3 | 40.3 |

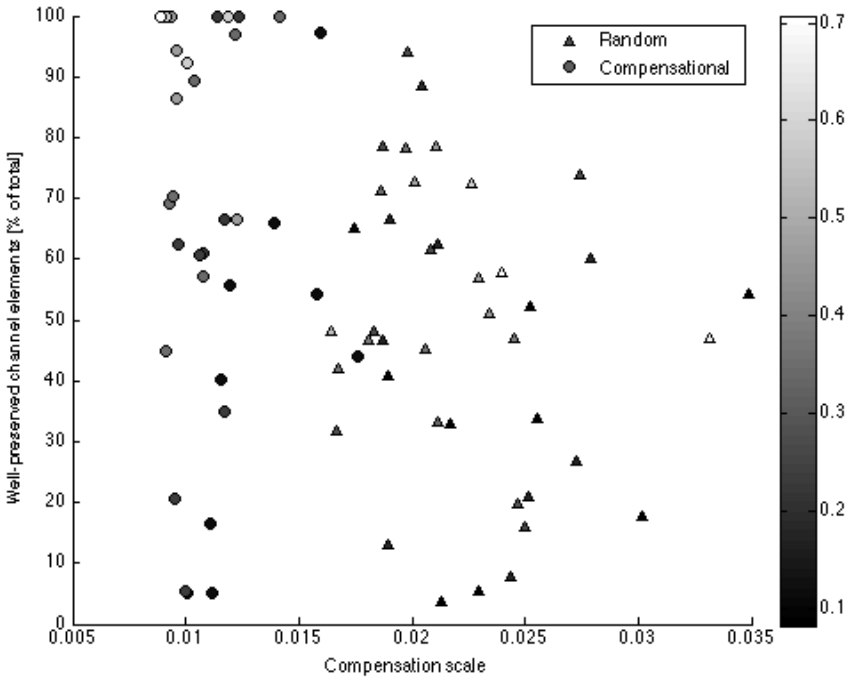


Figure DR7: Model results plotted against compensation scale rather than sediment retention (see manuscript Figure 3 for figure explanation). Compensation scale is the maximum thickness of autogenic dynamics (*Hmax* in Trampush et al. (2017) normalized by the stratigraphic thickness of the model run. The timescale of compensational avulsions is prescribed in the model runs (every channel goes to the lowest point in compensational model runs, and every $10^{th}$ channel is compensational in random model runs), so the compensational model have a much smaller compensation scale than the random models. There is no correlation between compensation scale and bar preservation for random or compensational models.

**REFERENCES**


Adams, M. M., and Bhattacharya, J. P., 2005, No Change in Fluvial Style Across a Sequence Boundary, Cretaceous Blackhawk and Castlegate Formations of Central Utah, U.S.A: Journal of Sedimentary Research, v. 75, no. 6, p. 1038-1051.

Chamberlin, E. P., 2016, Using stratigraphic architecture to isolate the role of avulsion processes in alluvial-basin filling [Ph.D.: The Pennsyvlania State University, 246 p.

Chamberlin, E. P., and Hajek, E. A., 2015, Interpreting Paleo-Avulsion Dynamics from Multistory Sand Bodies: Journal of Sedimentary Research, v. 85, no. 2, p. 82-94.

Fouch, T. D., Lawton, T. F., Nichols, D. J., Cashion, W. B., and Cobban, W. A., 1983, Patterns and timing of synorogenic sedimentation in Upper Cretaceous rocks of central and northeast Utah, *in* Reynolds, M. W., and Dolly, E. D., eds., Mesozoic Paleogeography of the West-Central United States: Denver, Rocky Mountain Section Society of Economic Paleontologists and Mineralogists, p. 305-336.

McLaurin, B. T., and Steel, R., 2000, Fourth-order nonmarine to marine sequences, middle Castlegate Formation, Book Cliffs, Utah: Geology, v. 28, no. 4, p. 359-362.

Miall, A., 2014, The Emptiness of the Stratigraphic Record: A Preliminary Evaluation of Missing Time In the Mesaverde Group, Book Cliffs, Utah, U.S.A: Journal of Sedimentary Research, v. 84, no. 6, p. 457-469.

Miall, A., and Arush, M., 2001, The Castlegate Sandstone of the Book Cliffs, Utah: Sequence Stratigraphy, Paleogeography, and Tectonic Controls: Journal of Sedimentary Research, v. 71, no. 4, p. 537-548.

Pattison, S., 2010, Alternative sequence stratigraphic model for the Desert Member to Castlegate Sandstone interval, Book Cliffs, eastern Utah: Implications for the high-resolution correlation of falling stage nonmarine, marginal-marine, and marine strata, *in* Morgan, L. A., and Quane, S. L., eds., Through the Generations: Geologic and Anthropogenic Field Exercusions in the Rocky Mountains from Modern to Ancient: Geological Society of America Field Guide 18, p. 163-192.

Robinson, R. A. J., and Slingerland, R. L., 1998, Grain-size trends, basin subsidence and sediment supply in the Campanian Castlegate Sandstone and equivalent conglomerates of central Utah: Basin Research, v. 10, p. 109-127.

Trampush, S. M., Hajek, E. A., Straub, K. M., and Chamberlin, E. P., 2017, Identifying autogenic sedimentation in fluvial-deltaic stratigraphy: Evaluating the effect of outcrop-quality data on the compensation statistic: Journal of Geophysical Research: Earth Surface, v. 122, no. 1, p. 91-113.

Van Wagoner, J. C., 1995, Sequence stratigraphy and marine to nonmarine facies architecture of foreland basin strata, Book Cliffs, Utah, U.S.A., *in* Van Wagoner, J. C., and Bertram, G. T., eds., Sequence Stratigraphy of Foreland Basin Deposits: Outcrop and Subsurface Examples from Cretaceous of North America, American Association of Petroleum Geologists, Memoir 64, p. 137-223.

Yoshida, S., 2000, Sequence and facies architecture of the upper Blackhawk Formation and the Lower Castlegate Sandstone (Upper Cretaceous), Book Cliffs, Utah, USA: Sedimentary Geology, p. 239-276.

Yoshida, S., Willis, A., and Miall, A., 1996, Tectonic Control of Nested Sequence Architecture in the Castlegate Sandstone (Upper Cretaceous), Book Cliffs, Utah: Journal of Sedimentary Research, v. 66, no. 4, p. 737-748.